33RD CONGRESS
OF THE INTERNATIONAL COUNCIL
OF THE AERONAUTICAL SCIENCES
STOCKHOLM, SWEDEN, 4-9 SEPTEMBER, 2022

ICAS 2022 SWEDEN

INFLUENCES OF CHANGING THE INSTALLING POSITIONS OF MULTIPLE WINGLETS ON AERODYNAMIC CHARACTERISTICS

Erina Kobayashi[1] & Kazuhisa Chiba[1]

[1]The University of Electro-Communications, 1-5-1, Chofugaoka, Chofu, Tokyo 182-8585, Japan

Abstract

This study investigated the influences on the aerodynamic characteristics by installing multiple winglets' positions on aircraft wingtips like primary feathers of birds. Multiple winglets contribute to the dispersion of the wingtip vortex and the reduction of induced drag but also help to improve lift by providing a suitable gap between the winglets. However, the previous study implemented a single installation position of multiple winglets on the main wing; the effects of the location relationship with the main wing on aerodynamic performance are unknown. Hence, we have conducted numerical analyses for two wing geometry patterns with three nonplanar winglets installed upwind and downwind for the wingtips. We additionally analyzed only the main wing for comparison. This study defines the winglets' position at the identical interval as those with the maximum lift coefficient in the previous research. Consequently, the multiple winglets restricted the wingtip vortex; both upwind-type and downwind-type models improved the lift-drag ratio of the main wing compared to the main wing alone. Furthermore, the lift-drag ratio of the main wing improved with upwind-type model than downwind-type one. But the negative pressure area on the main wing underside expanded in the spanwise direction due to intending the shock wave, which depends on the winglets' position. Thus, the lift-drag ratio of the whole wing decreased compared to that of the main wing alone. Future work aims to achieve aerodynamic performance superior to that of the single main wing by devising the airfoil shape of the main wing.

Keywords: Multiple winglets, Changing the Installation positions, Aerodynamic performance, Computational fluid dynamics

1. Introduction

Modern aircraft have been used to transport people and loads; it needs to improve fuel consumption to consider environmental issues dramatically. Aerodynamic drag reduction is a method to improve fuel efficiency. The drag is divided mainly into induced drag and entropy drag. The former always occurs at lift generation; the latter is not directly involved in lift generation. The reduction of induced drag significantly impacts aircraft performance because it accounts for roughly 25% of the total drag of a typical transport aircraft at cruise and about 60% at takeoff [1]. It is vital to disperse the wingtip vortex that causes air to flow from the lower surface to the upper surface due to the pressure difference of the wing surface [2]. Installing winglets is an effective way to do that. Winglets are tiny wings attached to the wingtips, and their shapes have been studied in various ways [3, 4, 5, 6].

Whitcomb [3] conducted wind tunnel tests at subsonic speeds with the winglets attached to the wingtips of the representative first-generation, narrow-body jet transport. He clarified that installing the winglets reduced the induced drag by roughly 20%; increased the lift-drag ratio L/D by approximately 9%. Also, there are studies on the design of winglets using geometrical parameters such as dihedral, twist, and sweep angles to the main wing [4, 5]. There are additional studies on split-tip winglet shapes with another small wing attached to the lower surface of the winglets [1, 7, 8, 9]. Reddy et al. [7, 8] revealed that the two tiny wings of the split-tip winglet diffused the wingtip vortex and reduced the drag by 4% compared to a single winglet.

Studies focusing on biomimicry have been conducted to improve the winglet performance further than the current winglets. Bird wings have multiple primary feathers, which form slits at the wingtip. It has been discovered that these slits allow each feather to stir independently, disperse the wingtip vortices and reduce the induced drag [10]. Thus, recent research has considered a geometry that mimics the characteristics of the birds' wingtips by placing multiple winglets in the chord direction on an aircraft's main wing [11, 12, 13, 14, 15]. These are called multi-winglets.

Smith et al. [11] carried out wind tunnel experiments with five planar winglets, five of each with a different angle of attack and dihedral angle to the main wing. It demonstrated that the vortex was dispersed into five vortices, the blowdown on the entire wing reduced, and the L/D increased up to 30% compared to the main wing alone. It likewise indicated that the active control of each winglet's angle of attack and dihedral angle could substitute for ailerons and relieve the impacts of wind gusts on the aircraft's stability [12]. Other studies have examined the effects of applying twist and sweep angles to multiple winglets [14] and adding more winglets to suppress wingtip vortices [16].

The fact that winglets also play a role in increasing lift is one of the adequate design strategies for commercial aircraft that would like to grow their operational efficiency as much as possible. The abilities of multi-winglets are not limited to the decrease in induced drag and improved stability. Lynch et al. [15] focused on the gaps between the winglets because raptors have slits between the primary feathers for a higher lift. They elucidated that the lift rises by setting a suitable gap width between the three winglets. This study also compared planar and non-planar winglets; the non-planar winglets diminished the induced drag more and clarified the effect of the gap width on the lift regardless of the winglet planarity.

The difference in the winglets' place in the upwind and downwind directions must ameliorate the correlation with the difference in the phenomenon of the wing chord direction, which must improve the aerodynamic performance. However, previous studies have focused on verifying the effectiveness of multi-winglets and have not yet examined the effect of winglets' position on the main wing. This study scrutinizes the impact of the multi-winglets' location relative to the main wing on the aerodynamic performance by comparing two cases: one installed at the very front and the other at the very rear. We would perform numerical simulations for configurations with three non-planar winglets installed at the upwind and downwind place of the main wing. The gap between the winglets is fixed at the gap size where the experiment of Lynch et al. [15] accomplished the maximum lift coefficient. Note that we would prepare a reference single-wing model (no winglets) as a comparison. In addition, this study aims not to mount the wing under verification on a pragmatic aircraft but to investigate the influences by changing multi-winglets positions; to assure the feasibility of multi-winglets. Hence, as the first step, we defined the main wing as a simple rectangular one.

This paper is organized as follows. Section 2 describes the numerical method, the wing numerical models, and the computational meshes. Section 3 discusses the differences in aerodynamic performance and their physical mechanisms from the analysis results obtained. Finally, section 4 summarizes the conclusions and prospects.

2. Problem definition

2.1 Configuration

The model geometry consists of the main wing and three non-planar winglets, as shown in Fig. 1. c_b and b_b represent the main wing's chord length and semi-span length, respectively red; c_t and b_t are the winglets' chord length and span length. The first, second, and third winglets are designated from the upwind side. OpenVSP [17] creates the geometry based on the wing used in [15]. However, since different Mach numbers M and Reynolds numbers Re are adopted as flight conditions, we modified the actual dimensions for the study. The present study decides the main wing and the winglets as follows:

- main wing
  It is defined as an untwisted rectangular airfoil with a cross-section of NACA0012. This study uses an airfoil without a camber because we focus only on the positional relationship between the multi-winglets and the main wing in the chord direction. We additionally round the wingtip to subdue the wingtip vortex. The chord length c_b is 7.500 m; the span length b_b is 15.625 m.

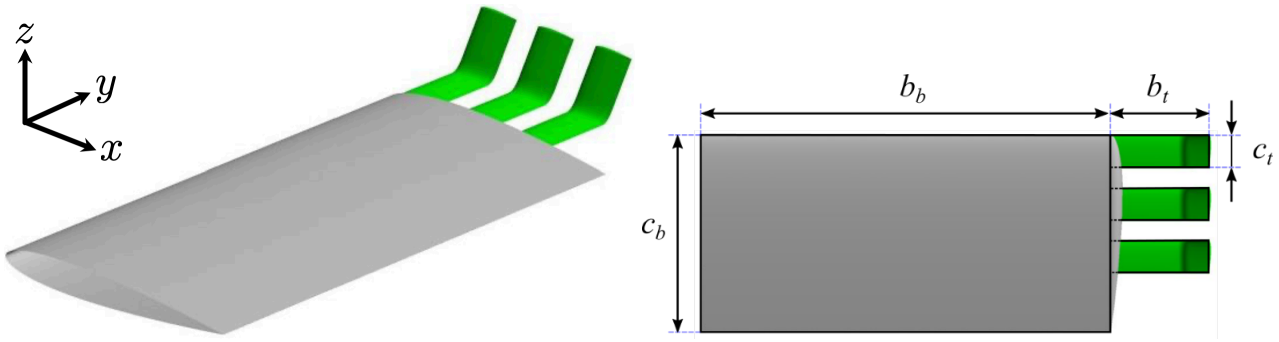

(a) Overview (b) Topview

Figure 1 – Configuration of the computational model.

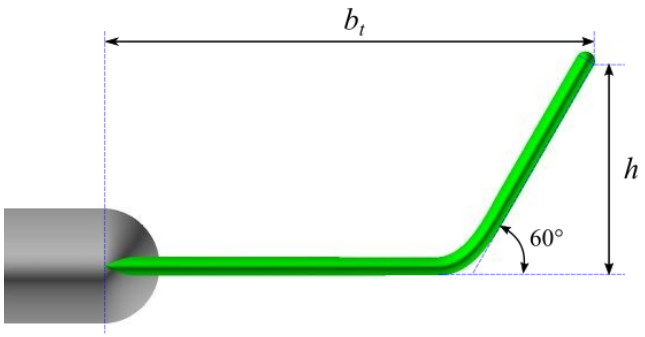

Figure 2 – Multi-winglets with non-planar geometry.

- winglets
  The main wing is designed with a non-planar geometry, as shown in Fig. 2, referring to [15]. As with the main wing, the NACA0012 airfoil shape is used for all three winglets, bent one part, respectively. The chord length c_t is 1.250 m, the span length b_t is 3.750 m, and the height h is defined by Eq. (1) [15].

$$h = (b_b + b_t) \times 0.075 \tag{1}$$

  The winglets are lined up so that the camber lines of the winglets and the main wings overlap. The gap between the winglets is fixed at 10% of c_b, which obtained the maximum lift coefficient C_L in [15]. The deflection angles to the main wings are all unified at 0°. We also round their wingtips as well as the main wing's wingtip.

The position of the three winglets to the main wing is simplified by defining just two patterns: the upwind- and the downwind-type winglets. The upwind-type aligns the leading edge of the first winglet with that of the main wing. The downwind-type places the third winglet 0.050 m forward of the main wing's trailing edge because the third winglet connects smoothly near the trailing edge of the main wing. Figure 3 shows the position of the first three winglets in the chord direction for each configuration (the main wing's leading edge corresponds with 0%; its trailing edge is 100%). Note that we analyze all configurations using half-cut models because crosswind conditions are not considered.

2.2 Mesh generations

We used MEGG3D (Multi-Element Grid Generation) [18, 19, 20, 21, 22, 23, 24, 25, 26, 27, 28], a software for automatically generating unstructured mesh. The computational space is a hemisphere with a radius of 15 times c_b. We apply prismatic layers in the vicinity of the object to grasp the boundary layer flow on the model surface. The maximum number of the prismatic layers is 40, the thickness of the first layer is $(100\sqrt{\mathrm{Re}})^{-1}$, and the stretching factor is set to 1.2 to ensure the resolution of the boundary layer. Table 1 compiles the number of mesh points for the present models' surfaces

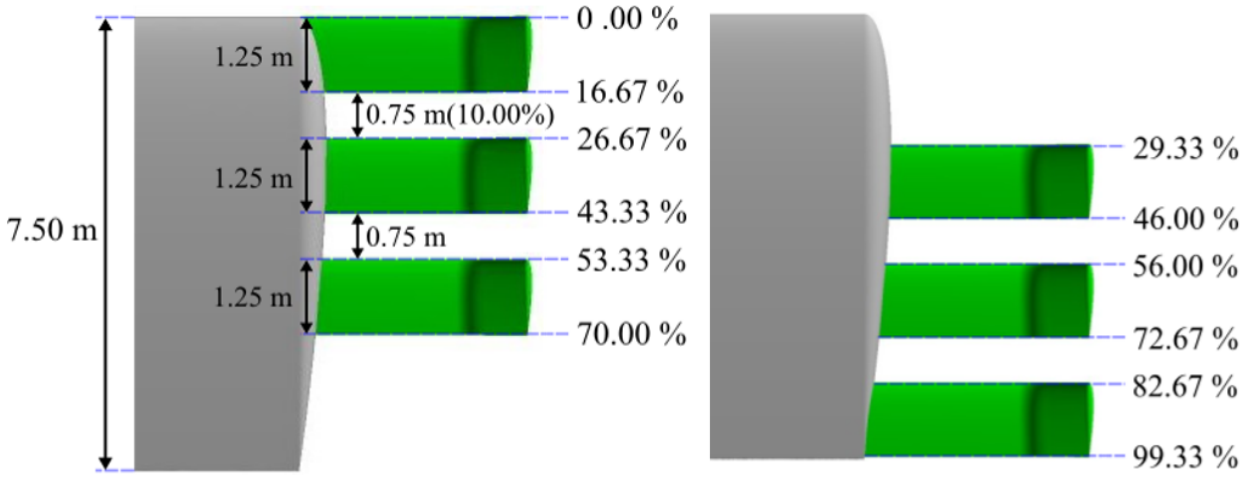

(a) upwind-type model (b) downwind-type model

Figure 3 – Position of the multi-winglets relative to the main wing.

Table 1 – Number of mesh points for the whole model surface and computational space.

model name	*model surface* (million)	*computational space* (million)
single-wing	0.36	15.7
upwind-type	0.52	22.6
downwind-type	0.53	22.8

and volumes for the single-wing, upwind-type, and downwind-type models. Preliminary numerical experiments analyzed the upwind-type model with three mesh densities (coarse, fine, and super-fine meshes). Since the C_D convergence difference was within 0.1 cts, we generated a computational mesh for all the present configurations with a mesh density comparable to the fine mesh.

2.3 Flow solver

We use compressible flow solver FaSTAR [29] developed by Japan Aerospace Exploration Agency. It solves the 3D Reynolds-averaged Navier-Stokes equations by an unstructured MUSCL-type cell-vertex finite volume method with Hishida's differentiable slope limiter for keeping second-order spatial accuracy. FaSTAR uses schemes: the Harten-Lax-van Leer-Einfeldt-Wada method [30] for numerical flux computations; the lower-upper symmetric-Gauss-Seidel [31] implicit scheme for time integration. This study adopts the Shear Stress Transport two-equation turbulence model [32]. Computations run on the cluster constructed of five nodes; one is with Intel Xeon E5-2660 2.2 GHz 16 core and 64 GB memory. It takes roughly 40 hours for one case at least.

2.4 Computational conditions

Since this study assumes the cruising condition of a commercial aircraft, the angle of attack is set to 3°. We specified M to 0.85 and C_b-based Re to 5.0×10^6 based on the conditions for NASA Common Research Model [33].

3. Results and discussion

This section clarifies the effect of the multiple winglets' attachment position by comparing the C_L, C_D, and L/D in Fig. 4. The results decompose the C_L and C_D of the upwind-type and downwind-type models into each element: the main wing, the first, second, and third winglets. Figure 4c also displays the L/D for each component. We would examine each aerodynamic performance. Figure 4 reveals the following points:

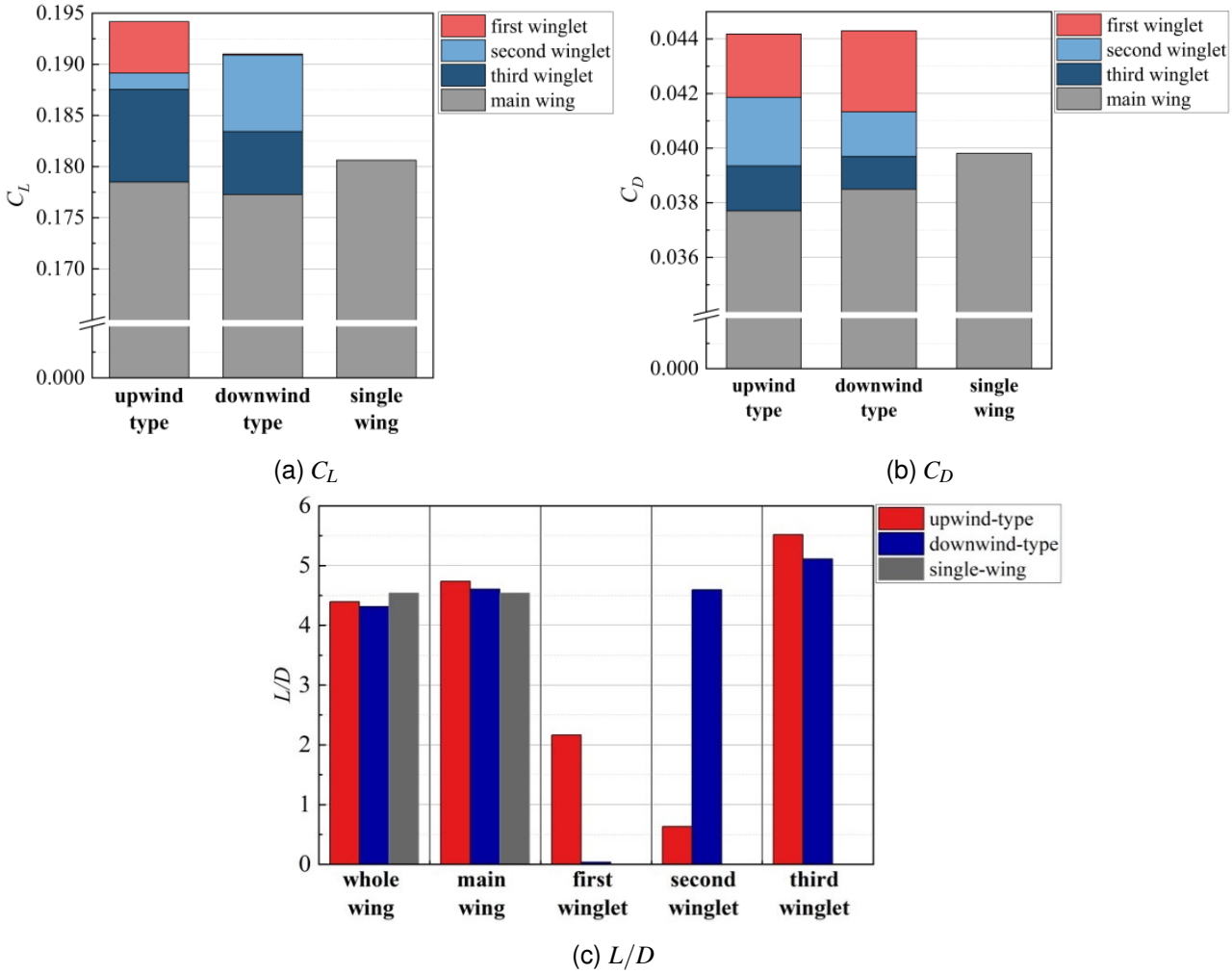

(a) C_L (b) C_D

(c) L/D

Figure 4 – Comparison of aerodynamic performance.

(1) The upwind-type model outperforms the downwind-type one in C_L, C_D, and L/D of the main wing and the whole wing. The flow field is habitually computed under the identical condition described in subsection 2.4.
(2) The second winglet in the upwind-type model has the lowest C_L among the three winglets; the first winglet in the downwind-type one has also the lowest C_L among the three winglets.
(3) Both the upwind-type and downwind-type models reduce the C_D of the main wing and improve the L/D of the main wing compared to the single-wing one.
(4) Both the upwind-type and downwind-type models decline L/D of the whole wing compared to the single-wing one.

Since (1) and (2) are influenced by the position of the multi-winglets, we will discuss them separately in the following two subsections on the upwind-type and downwind-type models below. Moreover, we divide them into two subsubsections focusing on the main wing and the multi-winglets. (3) and (4) are independent of the position of the multi-winglets and are the consequence of attaching them. Thus, in discussing the main-wing performance in the subsubsection of the upwind-type model, we compare it with the single-wing model without the multi-winglets; we debate (3) and (4) to reveal the influences of the presence/absence of the multi-winglets.
Figures 5 and 6 are used for the following discussion. Figure 5 visualizes the surface pressure coefficient C_p distribution to elucidate how the C_L varies in the main wing and multi-winglets. Figure 6 shows the C_p distribution in the y-z cross-section at 80% of the chordwise to investigate the multi-winglets' degree of wingtip vortex suppression.

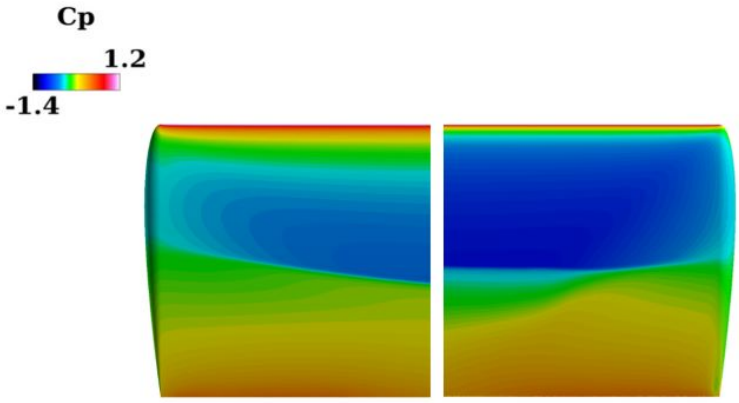

(a) single-wing model

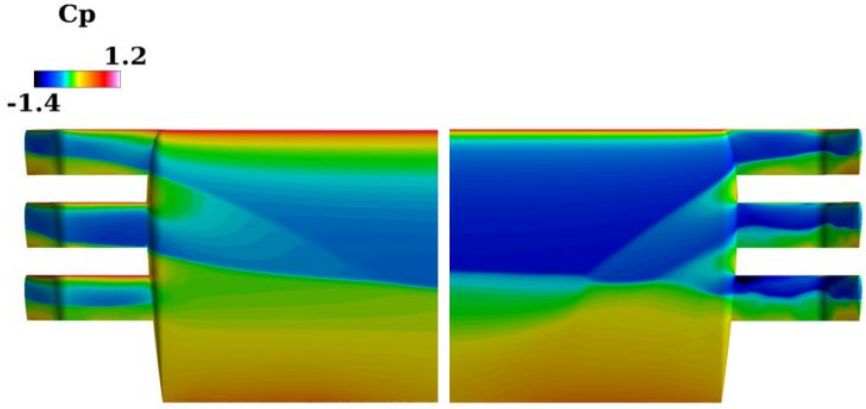

(b) upwind-type model

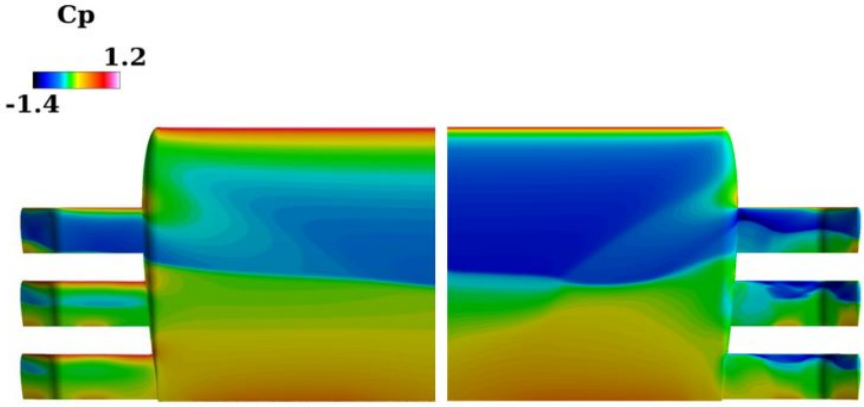

(c) downwind-type model

Figure 5 – Comparison of C_p distribution near the wingtip (left: lower surface, right: upper surface).

3.1 Upwind-type model

The aerodynamic effects of the multi-winglets attachment can be classified into those on the main wing and the multi-winglets. Accordingly, we will divide the discussion into the main wing and the multi-winglets subsubsections.

3.1.1 Main wing

- C_L: Figure 4a shows that the C_L of the upwind-type model is 1.2% lower than that of the single-wing model. To investigate the cause of this decrease, we would observe the pressure distribution on the model's surface.
  Figure 5a indicates the C_p distribution on the upper and lower surfaces of the single-wing model.

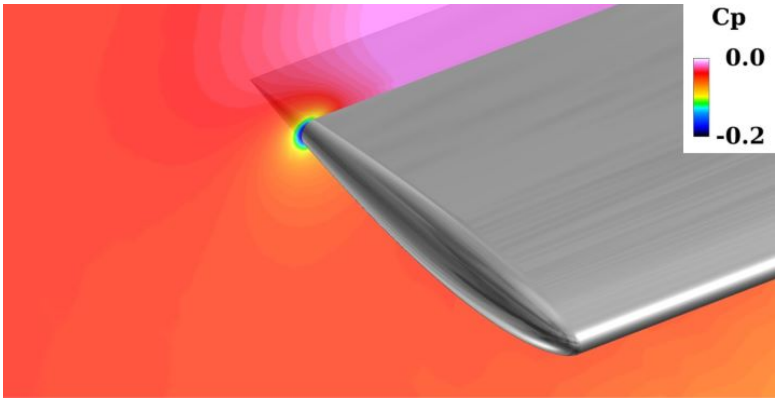

(a) single-wing model

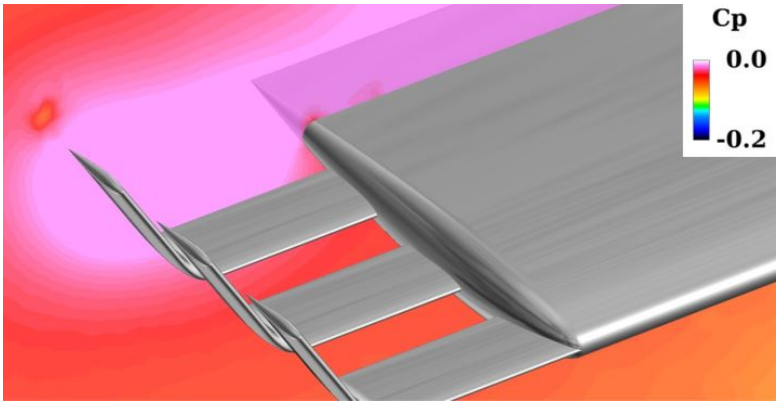

(b) upwind-type model

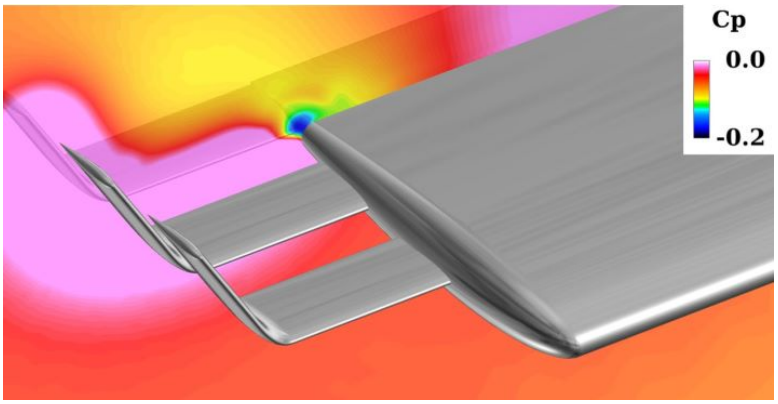

(c) downwind-type model

Figure 6 – C_p distribution on the 80% chordwise cross section.

From this figure, we can see that the pressure gradually recovers toward the wingtip. On the other hand, in the C_p distribution on the lower surface of the upwind-type model shown in Fig. 5b, the shock wave is split into two waves outside the 62% spanwise position of the main wing; each wave extends to the first and second winglets. In brief, the coupling of the shock waves generated by the main wing and the multi-winglets, respectively, locally prevents pressure recovery near the wing tip on the underside of the main wing.
In contrast, observing the pressure distribution on the top surface, Fig. 5b reveals that the shock waves on the main wing of the upwind-type model are separated at the 77% and 89% spanwise locations. In other words, on the upper surface of the main wing of the upwind-type model, the shock waves generated on the upper surfaces of the first, second, and third winglets merge with those rendered by the main wing. In the single-wing model, the negative pressure region

extends to the wingtip. However, the upwind-type model causes a high-pressure zone around the wingtip (gaps between each winglet) on the main wing surface. In particular, the intensity of the shock wave induced on the main wing top surface from the first winglet is vigorous; the pressure recovery behind the shock wave is one of the factors that cause the C_L to decline.

- C_D: Figure 4b is a graph of the integrated C_D values for each configuration. The upwind-type and downwind-type models have higher C_D due to the multi-winglets than the single-wing model. However, the C_D of the main wing panel alone tends to be lower than is the case without multi-winglets. In this subsection, we contrast the upwind-type and the single-wing models to examine the cause of the difference in the C_D value generated by the main wing.
  Figure 4b indicates that the main-wing's C_D value of the upwind-type model is 5.3% smaller than that of the single-wing model. Since the winglet plays a role in the wingtip vortex suppression effect, Fig. 6 depicts the flow structure near the wingtip. In the single-wing model shown in Fig. 6a, a negative pressure region appears near the wingtip, suggesting the growth of wingtip vortices. In contrast, in Fig. 6b, which shows the identical cross-section in the upwind-type model, there is no pressure drop; the formation of wingtip vortices is suppressed. This distinction must be one of the factors that cause the difference in C_D values.
  To investigate the mechanism by which the multi-winglets delay the generation of wingtip vortices, streamlines near the wingtip are depicted in Fig. 7. Figure 7a illustrates streamlines in the single-wing model, which flow along the wingtip wall toward the rear and into the main wing's upper surface due to the 3° angle of attack. In contrast, in Fig. 7b, which depicts the streamlines in the upwind-type model, the multi-winglets similarly obstruct the flow to the wing's upper surface as a result, reducing the flux over the main wing's upper surface stunts the wingtip vortex.
  However, the entropy drag must grow due to inflated volume if winglets are installed over the entire area from the leading edge to the trailing edge. Thus, we should consider the relationship between induced and entropy drags, which reduces the total C_D value the most. There should be an appropriate position to install multi-winglets that balance induced and entropy drags to diminish the total C_D value.

3.1.2 Multi-winglets

We would examine the influence of each winglet on C_L and C_D in the upwind-type model. Figures 4a and 4b indicate the winglets that minimize/maximize C_L and C_D are as follows:

- C_L
  - max: third winglet
  - min: second winglet
- C_D
  - max: second winglet
  - min: third winglet

The results reveal that the second winglet deteriorates both C_L and C_D. It is one of the reasons for the lower L/D of the whole wing in the upwind-type model than that in the single-wing model. Figure 5b shows that the shock-wave location on the underside of the second winglet is closer to the trailing edge than the other winglets; the negative pressure region is wider than the two different winglets. The possible reasons for this are two: (i) the shock wave on the second winglet's lower surface slid rearward due to the close distance to that of the main wing; (ii) the shock wave position moved rearward due to the increased flow rate on the underside of the second winglet provoked by the presence of the first winglet.
On the other hand, the shock wave on the upper surface of the second winglet is more forward and wavy than that of the first winglet (this tendency is even more pronounced for the third winglet). We ascribe it to the structure that the flow around the second winglet is disturbed by the first winglet and does not form a uniform flow (the effect is even more intensive for the third winglet because the flow is further disturbed). In other words, for effective utilization of the winglets after the second, it is

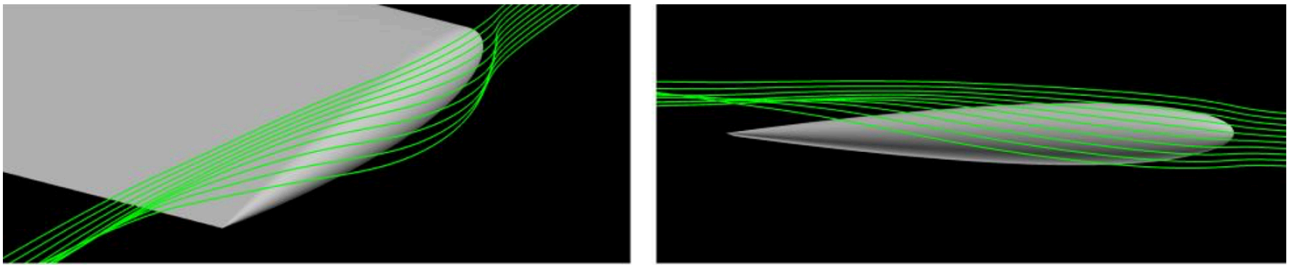

(a) single-wing model

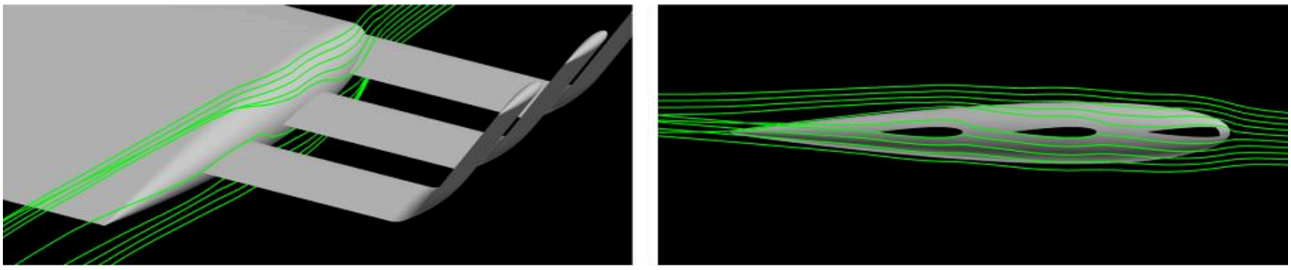

(b) upwind-type model

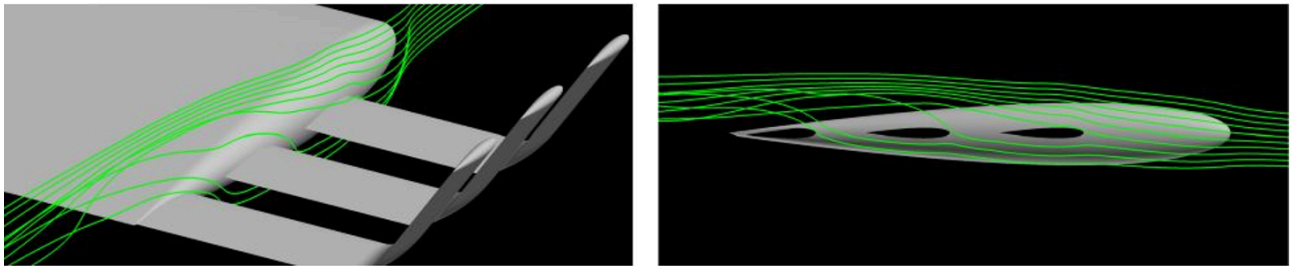

(c) downwind-type model

Figure 7 – Comparison of streamline around the wingtip between the single-wing, the upwind-type, and the downwind-type models (left: bird's eye view, right: side view).

essential to rectify the flow around them. Thus, we need to optimize the positional relationship of the attachment between each winglet.

3.2 Downwind-type model

This subsection discusses the downwind-type model following the argument of the upwind-type model in the previous subsection.

3.2.1 Main wing

- C_L: Figure 4a, which compares the C_L of the different models, demonstrates that the C_L of the downwind-type model is 0.7% lower than that of the upwind-type one. We would examine the cause of the decrease from the surface C_p distribution shown in Fig. 5c: On the underneath of the main wing in the downwind-type model, the shock wave induced by the wing extends and is connected with the shock wave rendered by the first winglet. Compared to the single-wing model, the downwind-type model has lower pressure near the wingtip where the first winglet is attached. However, the pressure drop range is narrower than in the upwind-type model.
  On the top surface, as on the bottom surface, only the shock wave by the first winglet is merged with the shock wave caused by the main wing. However, on the main wing top surface in the upwind-type model, the negative C_p region is broader than that of the downwind-type model because the shock waves generated by all winglets have combined with those of the main wing. These differences are the factors that produce the difference in C_L.

In the case of the downwind-type model, the first winglet is located aft of the main wing's leading edge, which causes a stagnation point in the uniform flow impinging on the first winglet. A high-pressure region is consequently formed near the first winglet on both the upper and lower surfaces of the main wing. It must be one of the causes for the lower C_L compared to the single-wing model. The first winglet should be located near the very front of the main wing to avoid this phenomenon.

- C_D: Figure 4b shows that the main-wing C_D in the downwind-type model grows by 2.1% compared to that in the upwind-type model. Figures 6b and 6c display that no negative C_p region arises in the upwind-type model due to the wingtip vortex at the 80% chordwise position. By contrast, a wingtip vortex has already formed over the main wing at the identical location for the downwind-type model. Hence, there is a difference in the degree of wingtip vortex suppression depending on the position of the multi-winglets. Furthermore, the C_D value of the whole wing is also higher for the downwind-type model than for the upwind-type one. Considering that vortices are likewise caused at the multi-winglet tips, the sum of the vorticity produced at both the main-wing and the multi-winglet tips should be less for the upwind-type model than the downwind-type one.
  Figure 7c, which visualizes the streamlines around the wingtip in the downwind-type model, is used to discuss this physical mechanism. Although the first winglet divides the streamlines, the flow rate at the underside of the winglet is less than in the upwind-type model. We ascribe it to the flow winding up between the main-wing leading edge and the first winglet. Compared to the single-wing model, the three winglets prevent the flow from winding up in the downwind-type model. However, the flow ahead of the first winglet has already rolled up, forming a wingtip vortex. In conclusion, the appropriate strategy is to inhibit the wingtip vortex core, which grows downstream from near the leading edge of the main wing, at an early stage.

3.2.2 Multi-winglets

Finally, we examine the role of each winglet in the downwind-type model. The contributions of the winglets to the C_L and C_D values can be summarized as follows:

- C_L
  - max: second winglet
  - min: first winglet
- C_D
  - max: first winglet
  - min: third winglet

This result reveals that the first winglet deteriorates both C_L and C_D, which is the main reason for the lower L/D of the downwind-type model. The shock wave is located rearward on the bottom of the first winglet due to mutual interference with the shock wave by the main wing shown in Fig. 5c. Therefore, the underside C_p decreases over almost the entire area, and a positive C_L cannot be generated.
In the case of the upper surface, the first winglet lies rearward of the leading edge of the main wing; it is subjected to flow turbulence around the wingtip so that the area around the winglet root does not function as a wing. The lower surfaces after the second winglet are not affected by the wing shock wave and retain a higher pressure than the upwind-type model. On the upper surface, however, the growth of wingtip vortices and turbulence in the wake of the first winglet hinder the function of the winglets, resulting in a lower C_L.
Thus, the first winglet should be placed near the leading edge of the main wing; the first-winglet airfoil shape should be designed to straighten its wake. After the second winglet, the slits between the winglets should be arranged to accelerate the flow from the lower to the upper surface while avoiding interference with the main-wing shock wave.

3.3 Future studies

Intuitive design strategies to improve L/D of multi-winglets configurations are to raise C_L and diminish C_D of the main wing and multi-winglets. This paper, which aims to prove the efficacy of the multi-winglets concept in ameliorating L/D over a single-wing model, has resulted in several findings that will enhance overall wing performance. Based on these, the usefulness of each of the above design strategies can be discussed as follows:

(1) To grow the main-wing C_L, which lowers by the multiple winglets:
This redesign effectively improves the L/D because the main-wing C_L reduction is the largest. In the case of upwind-type configurations, the main-wing C_L reduction is caused by the shock waves extending from each winglet, so it is desirable to design a winglets geometry that relieves the shock-wave generations on the winglets.

(2) To raise C_L from the multi-winglets:
It is expected that the L/D in each winglet can be independently enhanced by optimally designing the geometries of each winglet, defined as a 3D shape with neither twist nor sweep angle, using the NACA0012 symmetric airfoil model in the present study. However, the contribution of the multi-winglets L/D to the overall L/D is smaller than that of the main wing. Thus, the effect must be slight.
On the other hand, it is skeptical that the gap between winglets is productive enough to reduce the pressure on the top surface of the winglets by accelerating the flow; optimization of the winglet configuration is anticipated to be a helpful design strategy.

(3) To trim the main-wing C_D by the multi-winglets:
It is conceivable to augment the wingtip vortex suppression effect of the main wings from the current state by extending the chord length of each winglet and attaching them from the leading edge to the trailing edge of the wingtip. This method can prevent flow roll-up and diminish induced drag, but it cannot be a practical design measure because it simultaneously grows the entropy drag. Nonetheless, this is a relevant comparison case; multi-winglets anticipate to be better than a simple extension of the original main wing, which must undoubtedly be beneficial.

(4) To reduce C_D in the multi-winglets:
Lowering the volume of each winglet can decline the entropy drag. However, this decrease grows the induced drag of the main wing, so there is a tradeoff with the design strategy in (3); an optimal design that minimizes the total C_D is essential.

4. Conclusions

This study has investigated the effects of changing the installation position of multiple winglets on the aerodynamic performance of multi-winglet configurations; we compared the aerodynamic performance of three winglets installed upwind and downwind with that of a single wing. As a result, it was found that the upwind-type model improved the aerodynamic performance of the main wing more than the downwind-type one. We attribute it to the mechanism that the winglets at the upwind place of the main wing restrict the flow from the lower surface to the upper surface of the wing at an early stage and reduce the wingtip vortices over the main wing. However, the multi-winglets themselves diminish the lift-drag ratio of the whole wing. This mechanism is that the position of the winglets to the main wing extends the shock waves generated by the main wing and expands the negative pressure area of the winglets, especially on the lower surface.

Acknowledgment

FieldView20 created whole CFD visual images, which FieldView CFD, Inc. provides via its University Partners Program.

Contact Author Email Address

mailto: k2232054@edu.cc.uec.ac.jp

Copyright Statement

References

[1] T. S, Y. W, and Y. T, "Drag/weight reduction using split-tip winglet for TRA2012A model," *Transactions of the Japan society for aeronautical and space sciences*, vol. 63, no. 3, pp. 69–79, 2020.

[2] M. Segui, F. A. Roberto, R. M. Botez, and A. Ceruti, "New aerodynamic studies of an adaptive winglet application on the regional jet CRJ700," *Biomimetics*, vol. 6, no. 54, pp. 1–22, 2021.

[3] R. T. Whitcomb, "A design approach and selected wind tunnel results at high subsonic speeds for wingtip mounted winglets," NASA, Technical Note D-8260, 1976.

[4] M. D. Maughmer, "Design of winglets for high-performance sailplanes," *Journal of Aircraft*, vol. 40, no. 6, pp. 1099–1106, 2003.

[5] K. Takenaka, K. Hatanaka, W. Yamazaki, and K. Nakahashi, "Multidisciplinary design exploration for a winglet," *Journal of Aircraft*, vol. 45, no. 5, pp. 1601–1611, 2008.

[6] S. A. Ning and I. Kroo, "Multidisciplinary considerations in the design of wings and wing tip devices," *Journal of Aircraft*, vol. 47, no. 2, pp. 534–543, 2010.

[7] S. R. Reddy, H. Sobieczky, A. B. A. S. Adboli, and G. S. Dulikravich, "Winglets-multiobjective optimization of aerodynamic shapes," in *Proceedings in 11th World Congress on Computational Mechanics*. WCCM, 2014.

[8] S. R. Reddy, A. Neiss, and S. Powell, "Design, analysis and multi-objective constrained optimization of multi-winglets," Ph.D. dissertation, Mechanical and Materials Engineering Department, Florida International University, Miami, FL, USA, 2014.

[9] P. Bourdin, A. Gatto, and M. Friswell, "Potential of articulated split wingtips for morphing-based control of a flying wing," in *AIAA Paper 2007-4443 on 25th AIAA Applied Aerodynamics Conference*. AIAA, 2007.

[10] V. A. Tucker, "Drag reduction by wing tip slots in a gliding harris' hawk, parabuteo unicinctus," *The Journal of Experimental Biology*, vol. 198, no. 3, pp. 775–781, 1995.

[11] M. J. Smith, N. Komerath, R. Ames, O. Wong, and J. Pearson, "Performance analysis of a wing with multiple winglets," in *AIAA Paper 2001-2407 on 19th AIAA Applied Aerodynamics Conference*. AIAA, 2001.

[12] A. Shelton, A. Tomar, J. V. R. Prasad, M. J. Smith, and N. Komerath, "Active multiple winglets for improved unmanned-aerial-vehicle performance," *Journal of Aircraft*, vol. 43, no. 1, pp. 110–116, 2006.

[13] D. S. Miklosovic, "Analytic and experimental investigation of dihedral configurations of three-winglet planforms," *Journal of Fluids Engineering*, vol. 130, no. 7, p. 071103, 2008.

[14] M. Fluck and C. Crawford, "A lifting line model to investigate the influence of tip feathers on wing performance," *Bioinspiration & Biomimetics*, vol. 9, no. 4, p. 046017, 2014.

[15] M. Lynch, B. Mandadzhiev, and A. Wissa, "Bioinspired wingtip devices: A pathway to improve aerodynamic performance during low Reynolds number flight," *Bioinspiration & Biomimetics*, vol. 13, no. 3, p. 036003, 2018.

[16] Z. Hui, G. Cheng, and G. Chen, "Experimental investigation on tip-vortex flow characteristics of novel bionic multi-tip winglet configurations," *Physics of Fluids*, vol. 33, no. 1, p. 011902, 2021.

[17] A. S. Hahn, "Vehicle sketch pad: A parametric geometry modeler for conceptual aircraft design," in *AIAA Paper 2010-0657 on 48th AIAA Aerospace Sciences Meeting*. AIAA, 2010.

[18] Y. Ito and K. Nakahashi, "Direct surface triangulation using stereolithography data," *AIAA Journal*, vol. 40, no. 3, pp. 490–496, 2002.

[19] ——, "Surface triangulation for polygonal models based on CAD data," *International Journal for Numerical Methods in Fluids*, vol. 39, no. 1, pp. 75–96, 2002.

[20] ——, "Improvements in the reliability and quality of unstructured hybrid mesh generation," *International Journal for Numerical Methods in Fluids*, vol. 45, no. 1, pp. 79–108, 2004.

[21] Y. Ito, A. M. Shih, and B. K. Soni, "Reliable isotropic tetrahedral mesh generation based on an advancing front method," in *Proceedings of the 13th International Meshing Roundtable*, Williamsburg, VA, 2004, pp. 95–105.

[22] Y. Ito, A. M. Shih, B. K. Soni, and K. Nakahashi, "Multiple marching direction approach to generate high quality hybrid meshes," *AIAA Journal*, vol. 45, no. 1, pp. 162–167, 2007.

[23] Y. Ito, A. M. Shih, and B. K. Soni, "Octree-based reasonable-quality hexahedral mesh generation using a new set of refinement templates," *International Journal for Numerical Methods in Engineering*, vol. 77, no. 13, pp. 1809–1833, 2009.

[24] Y. Ito, M. Murayama, K. Yamamoto, A. M. Shih, and B. K. Soni, "Efficient computational fluid dynamics evaluation of small device locations with automatic local remeshing," *AIAA Journal*, vol. 47, no. 5, pp. 1270–1276, 2009.

[25] Y. Ito, A. M. Shih, R. P. Koomullil, N. Kasmai, M. Jankun-Kelly, and D. Thompson, "Solution adaptive mesh generation using feature-aligned embedded surface meshes," *AIAA Journal*, vol. 47, no. 8, pp. 1879–1888, 2009.

[26] Y. Ito, M. Murayama, K. Yamamoto, A. M. Shih, and B. K. Soni, "Efficient hybrid surface and volume mesh generation for viscous flow simulations," in *AIAA Paper 2011-3539 on 20th AIAA Computational Fluid Dynamics Conference*, 2011.

[27] Y. Ito, A. M. Shih, and B. K. Soni, "Three dimensional automatic local remeshing for two or more hybrid meshes," *International Journal for Numerical Methods in Fluids*, vol. 66, no. 12, pp. 1495–1505, 2011.

[28] ——, "Hybrid mesh generation with embedded surfaces using a multiple marching direction approach," *International Journal for Numerical Methods in Fluids*, vol. 67, no. 1, pp. 1–7, 2011.

[29] A. Hashimoto, K. Murakami, T. Aoyama, K. Ishiko, M. Hishida, M. Sakashita, and P. R. Lahur, "Toward the fastest unstructured CFD code "FaSTAR"," in *AIAA Paper 2012-1075 on 50th AIAA Aerospace Science Meeting*, 2012.

[30] S. Obayashi and G. P. Guruswamy, "Convergence acceleration of an aeroelastic Navier-Stokes solver," *AIAA Journal*, vol. 33, no. 6, pp. 1134–1141, 1994.

[31] D. Sharov and K. Nakahashi, "Reordering of hybrid unstructured grids for lower-upper symmetric Gauss-Seidel computations," *AIAA Journal*, vol. 36, no. 3, pp. 484–486, 1998.

[32] F. R. Menter, "Two-equation eddy-viscosity turbulence models for engineering applications," *AIAA Journal*, vol. 32, no. 8, pp. 1598–1605, 1994.

[33] M. B. Rivers, "NASA common research model: A history and future plans," in *AIAA Paper 2019-3725 on the AIAA Aviation 2019 Forum*. AIAA, 2019.